DOI: 10.1002/chem.200701252

Hypervalent Silicon versus Carbon: Ball-in-a-Box Model

Simon C. A. H. Pierrefixe, Célia Fonseca Guerra, and F. Matthias Bickelhaupt*[a]

Abstract: Why is silicon hypervalent and carbon not? Or why is $[Cl{-}CH_3{-}Cl]^-$ labile with a tendency to localize one of its axial C–Cl bonds and to largely break the other one, while the isostructural and isoelectronic $[Cl{-}SiH_3{-}Cl]^-$ forms a stable pentavalent species with a delocalized structure featuring two equivalent Si–Cl bonds? Various hypotheses have been developed over the years focusing on electronic and steric factors. Here, we present the so-called ball-in-a-box model, which tackles hypervalence from a new perspective. This model reveals the key role of steric factors and provides a simple way of understanding the above phenomena in terms of different atom sizes. Our bonding analyses are supported by computation experiments in which we probe, among other things, the shape of the S_N2 potential-energy surface of Cl^- attacking a carbon atom in the series of substrates CH_3Cl, $^{\bullet}CH_2Cl$, $^{\bullet\bullet}CHCl$, and $^{\bullet\bullet\bullet}CCl$. Our findings for $ClCH_3Cl^-$ and $ClSiH_3Cl^-$ are generalized to other Group 14 central atoms (Ge, Sn, and Pb) and axial substituents (F).

Keywords: bond theory · carbon · density functional calculations · hypervalent compounds · silicon · steric repulsion

Introduction

The concept of hypervalence has been challenging chemists for about a century.[1] Through the decades, the hypervalence or nonhypervalence of various atoms in both molecular as well as extended structures has been investigated.[2,3] However, also the definition and meaningfulness of the very concept itself has been the subject of, at times, vigorous discussions.[4,5] Here, we will not enter into such a discussion. The issue which we wish to address is the different bonding capabilities of two Group 14 atoms, carbon and silicon: why does carbon (as illustrated below) not bind more than four ligands[6] (except in some exotic or controversial examples[2,7,8]) while silicon (see below), despite being isoelectronic, can bind five[2,8,9] (or sometimes six, or even more[2,10]) substituents?

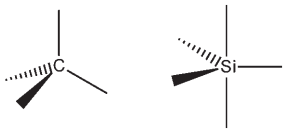

The above question also provides us with a robust and intuitive definition of hypervalence, rooted in experimental (and computational) observation, as being the capability of silicon (as opposed to the incapability of carbon) to exceed its "normal" tetravalence and form pentavalent, trigonal-bipyramidal species.

The nonhypervalence of carbon and the hypervalence of silicon are exemplified by the pentavalent D_{3h}-symmetric species $ClCH_3Cl^-$ (**1a**) and $ClSiH_3Cl^-$ (**2a**). While the former has a first-order saddle point that is labile towards localization of one C–Cl bond and (largely) towards breaking the other one, the latter is a stable pentavalent species. This is well known, since these species feature as the transition state and the stable transition complex in the intensely studied nucleophilic substitution reactions of $Cl^- + CH_3Cl$ (S_N2@C)[11–13] and $Cl^- + SiH_3Cl$ (S_N2@Si),[9,13–16] respectively (see Figure 1). Recently, we analyzed these reactions in terms of the rigidity and mutual interaction of the *reactants* (i.e., the nucleophile and the substrate) using the Activation Strain model.[16] It was shown that the crucial factor for having a central barrier for the S_N2@C and, thus, a labile pentavalent carbon atom, is mainly due to the increased steric repulsion between the nucleophile and the substituents. The central barrier disappears in the S_N2@Si reaction, because the larger distance between the nucleophile and the substituents reduces this steric repulsion. Moreover, in line

[a] S. C. A. H. Pierrefixe, Dr. C. Fonseca Guerra, Dr. F. M. Bickelhaupt
Theoretische Chemie
Scheikundig Laboratorium der Vrije Universiteit
De Boelelaan 1083, NL-1081 HV Amsterdam (The Netherlands)
Fax: (+31) 20-5987-629
E-mail: FM.Bickelhaupt@few.vu.nl

Supporting information for this article is available on the WWW under http://www.chemeurj.org/ or from the author.

with this steric picture, the central barrier can again be reintroduced in S_N2@Si reactions if the equatorial substituents are made more sterically demanding.[16]

In the present study, we wish to approach the phenomenon of hypervalency from a different perspective. Instead of a description of **I** in terms of the two S_N2 reactants **II**, we aim to understand the lability of five-coordinate carbon and the stability of pentavalent silicon in terms of the central carbon versus silicon atom interacting with the five surrounding (also mutually interacting) substituents **III**.

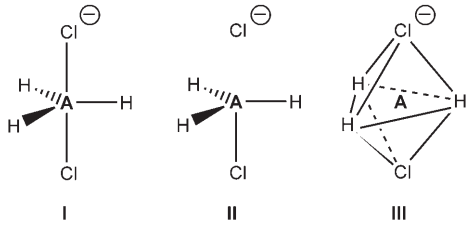

Of course, the description of **I** in terms of **II** is, ultimately, equivalent to the description of **I** in terms of **III**. It appears, however, that the alternative description **III** offers a simple and transparent way of understanding hypervalence (which we designate the "ball-in-a-box" model) that complements and integrates previous models of hypervalency.

Thus, we have analyzed the bonding in $ClCH_3Cl^-$ (**1**) and $ClSiH_3Cl^-$ (**2**) as well as in fragments thereof, such as, the "box" of five substituents that "contain" the central C or Si atom, using the Amsterdam Density Functional (ADF) program at the BP86/TZ2P level of density functional theory (DFT).[17,18] The analyses were carried out not only in the geometries of the various species that correspond to the D_{3h}-symmetric **1a** and **2a** (see Figure 2), but also along various deformation modes. First, we analyzed how the bonding changes if one proceeds from the symmetric species along the localization coordinate ζ, which for **1** and **2** are associated with a convex and concave potential-energy surface (PES), respectively (see Figure 1). Another deformation mode corresponds to the symmetric Cl–A–Cl stretch. Our bonding analyses are augmented (and supported) by computational experiments in which we probe, among other things, the shape of the S_N2 potential-energy surface of Cl^- attacking a carbon atom in the series of substrates CH_3Cl, $^{\bullet}CH_2Cl$, $^{\bullet\bullet}CHCl$ and $^{\bullet\bullet\bullet}CCl$. The findings for **1** and **2** were generalized by examining other Group 14 central atoms (germanium, tin, and lead, in which case relativistic effects were treated using the zeroth-order regular approximation (ZORA)[17r]) and axial substituents (fluorine).

The bonding analyses consisted of a decomposition of the total energy into interaction energies between (and within) fragments of the overall model systems **1** and **2**. The trends

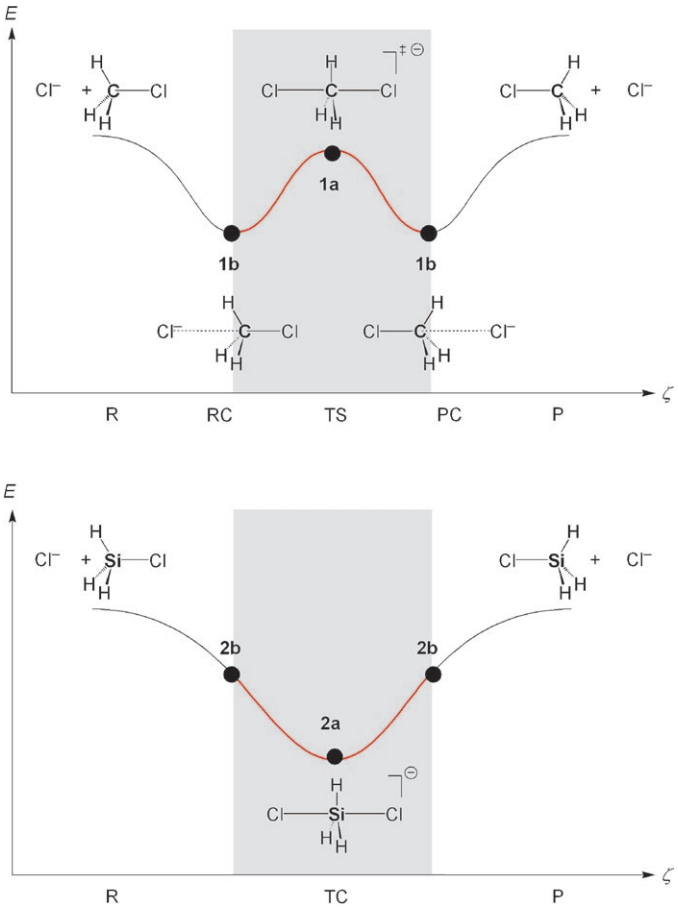

Figure 1. Double-well S_N2@C (upper) and single-well S_N2@Si (lower) potential-energy surfaces along the reaction coordinate ζ (R = reactants, RC = reactant complex, TS = transition state, TC = stable transition complex, PC = product complex, P = products).

Abstract in German: *Wieso ist Silizium hypervalent und Kohlenstoff nicht? Oder, warum ist [Cl–CH_3–Cl]$^-$ labil mit der Neigung eine seiner axialen C–Cl-Bindungen zu lokalisieren und die andere großenteils zu brechen, während das gleichförmige und isoelektronische [Cl–SiH_3–Cl]$^-$ eine stabile pentavalente Spezies bildet, mit einer delokalisierten Struktur, die durch zwei equivalente Si–Cl-Bindungen charakterisiert wird? Bisher wurden verschiedene Hypothesen entwickelt, die sich auf sterische oder aber auch auf elektronische Faktoren konzentrieren. Wir präsentieren hier das Ball-in-a-Box-Modell, in dem Hypervalenz aus einer neuen Perspektive angegangen wird. Das Ball-in-a-Box-Modell deckt die Schlüsselrolle der sterischen Faktoren auf und bietet einen zugänglichen Weg die obigen Phänomene anhand von unterschiedlichen Größen der Atome zu verstehen. Unsere Bindungsanalysen werden von numerischen Experimenten unterstützt, in denen wir unter anderen die Gestallt der Potentialoberflächen erkunden für die S_N2-Reactionen von Cl^- mit den Substraten CH_3Cl, $^{\bullet}CH_2Cl$, $^{\bullet\bullet}CHCl$ und $^{\bullet\bullet\bullet}CCl$. Wir zeigen, dass unser Modell für $ClCH_3Cl^-$ und $ClSiH_3Cl^-$ auch auf Systeme mit anderen Zentralatomen der Gruppe-14 (Ge, Sn and Pb) und anderen axialen Substituenten (F) übertragen werden kann.*

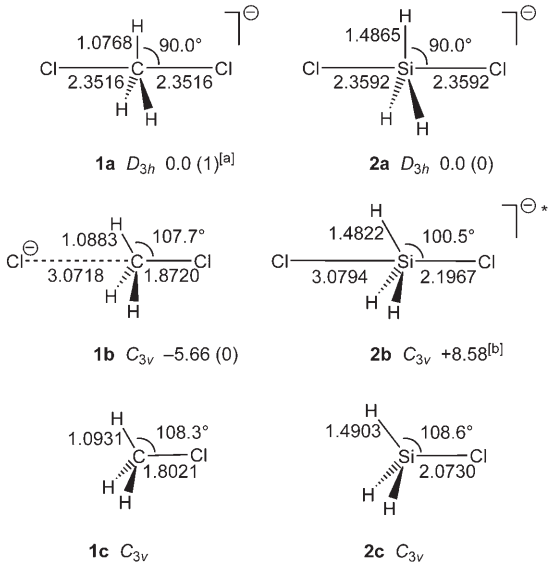

1a D_{3h} 0.0 (1)[a] **2a** D_{3h} 0.0 (0)

1b C_{3v} –5.66 (0) **2b** C_{3v} +8.58[b]

1c C_{3v} **2c** C_{3v}

Figure 2. Geometries (in Å, °), relative energies (in kcal mol^{-1}) and number of imaginary frequencies (in parentheses) of selected carbon (**1a–c**) and silicon (**2a–c**) structures, computed at BP86/TZ2P. [a] *i*316 cm^{-1}. [b] **2b** is *not* a stationary point (see text).

in the various energy terms were interpreted in the conceptual framework provided by the quantitative molecular orbital (MO) model contained in Kohn–Sham DFT.[18]

Qualitative MO analyses of pentacoordination were carried out in the early seventies by Hoffmann and co-workers,[19] who arrived at a bonding mechanism that naturally incorporates the 3-center–4-electron (3c-4e) bond proposed by Pimentel and Rundle[20] to account for the hypervalency of the central atom in species such as F_3^- and XeF_2. Originally, the 3c-4e bond was formulated in terms of the valence p_σ atomic orbitals (AOs) of a linear arrangement of three atoms that yields a well-known pattern of three MOs: ψ_1, ψ_2, and ψ_3, shown in Scheme 1. These MOs are bonding,

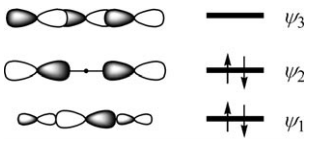

Scheme 1. MOs involved in 3c-4e bonding

nonbonding, and antibonding, respectively, with four electrons occupying ψ_1 and ψ_2.[21,22] This bonding pattern was confirmed by ab initio calculations, which showed that the central atom in the hypervalent species predominantly invokes its s and p AOs for bonding and that the d AOs merely act as corrective polarization functions, but not as valence orbitals.[23] These and other results have falsified Pauling's (plausible but, in the end, incorrect) hypothesis that the hypervalence of main group atoms such as silicon is derived from the availability of low-energy d AOs. These findings were confirmed by the present study and will not be discussed further.

Note that, while the 3c-4e MO model is a good description of the bonding in hypervalent species, it does not explain *why* such a bonding mechanism leads to stable hypervalent species in the case of silicon as the central atom but *not* in the case of carbon. On the other hand, in a valence bond (VB) study of the model systems CH_5^- and SiH_5^-, Hiberty, Shaik, and co-workers[24] were able to provide a qualitative explanation based on curve-crossing diagrams of VB configurations. They showed that the comparatively low-energy σ* orbitals of the equatorial Si–H bonds can accommodate the fifth valence-electron pair which, in the 3c-4e MO model of Scheme 1, corresponds to a stabilization of ψ_2. The σ* orbitals of the equatorial C–H bonds do not possess this capability (they are too high in energy). This results in a long axial H–C–H linkage and a high energy for CH_5^- relative to CH_4+H^-.

The ball-in-a-box model presented herein allows MO theory to, in a sense, catch up with VB theory regarding the treatment and understanding of why certain atoms (such as silicon) can form stable hypervalent configurations and others (such as carbon) cannot. The qualitative picture that emerges is of the five substituents forming a cage or a "box" (in which they are in mutual steric contact) and the central atom is a "ball" in that box. Silicon fits nearly exactly into this box and can bind simultaneously to the top and the bottom. At variance, the carbon atom is too small to touch both the top and the bottom of the box, and it can, thus, only bind to one of them. In this way, our ball-in-a-box model nicely integrates the bonding ("electronic factors") and repulsive features ("steric factors") in the bonding mechanism and highlights the importance of the relative size of the central atom.[4,13,15]

Computational Methods

All calculations were performed by using the Amsterdam Density Functional (ADF) program developed by Baerends et al.[17] The numerical integration was performed with the procedure developed by te Velde et al.[17g,h] The MOs were expanded in a large uncontracted set of Slater-type orbitals (STOs) containing diffuse functions: TZ2P (no Gaussian functions were involved).[17i] The basis set was of triple-ζ quality for all atoms and was augmented with two sets of polarization functions (i.e., 2p and 3d on H; 3d and 4f on C and F; 4d and 5f on Si and Cl; 4d and 4f on Ge; 5d and 4f on Sn; 6d and 5f on Pb). Core shells were treated using the frozen-core approximation (1s for C and F; 1s2s2p for Si and Cl; 1s2s2p2s3p for Ge; 1s2s2p2s3p3d4s4p for Sn; 1s2s2p2s3p4s4p4d for Pb).[17c] An auxiliary set of s, p, d, f and g STOs was used to fit the molecular density and to represent the Coulomb and exchange potentials accurately in each self-consistent field cycle.[17j]

Equilibrium structures were optimized by using analytical gradient techniques.[17k] Geometries, energies, and vibrational frequencies were computed at the BP86 level of the generalized gradient approximation (GGA). The exchange was described by Slater's Xα potential[17l] with corrections due to Becke[17m,n] added self-consistently and the correlation was treated by using the Vosko–Wilk–Nusair (VWN) parameterization[17o] with nonlocal corrections due to Perdew[17p] added self-consistently.[17q] For species containing Ge, Sn, or Pb, relativistic effects were treated by using the zeroth-order regular approximation (ZORA).[17r]

The bonding in $ClCH_3Cl^-$, $ClSiH_3Cl^-$, and other species was analyzed by using the quantitative molecular orbital (MO) model contained in the Kohn–Sham DFT.[18,25,26]

Results and Discussion

Structures and potential-energy surfaces: Consistent with previous work (see Figure 1 and the introduction), we found that D_{3h}-symmetric pentacoordinate $ClCH_3Cl^-$ (**1a**) is labile towards localization of one and elongation of the other C–Cl bond (i.e. a first-order saddle-point on the PES), whereas D_{3h}-symmetric $ClSiH_3Cl^-$ (**2a**) constitutes a stable pentavalent species (see Figure 2). An important observation, as will become clear later on, is that the C–Cl bonds (2.3516 Å) in the carbon species **1a** have nearly the same length as the Si–Cl bonds (2.3592 Å) in the silicon species **2a** (see Figure 2).

The localized C_{3v}-symmetric equilibrium structure $Cl^-\cdots CH_3Cl$ (**1b**) is 5.7 kcal mol^{-1} more stable than trigonal bipyramid **1a** (see Figure 2). For the silicon system, there is no such stationary point corresponding to a localized structure $Cl^-\cdots SiH_3Cl$ with a short and a long Si–Cl bond. However, for the purpose of comparison, we have computed the geometry and energy of a localized $Cl^-\cdots SiH_3Cl$ species (**2b**) that, although it is not a stationary point, closely resembles $Cl^-\cdots CH_3Cl$ (**1b**) in that one Si–Cl bond has been elongated, relative to the pentavalent **2a**, by the same amount (i.e. by 0.7202 Å) as the long C–Cl bond in **1b** relative to the pentavalent **1a** (see Figure 1). Thus, **2b** is obtained through optimizing $Cl^-\cdots SiH_3Cl$ in C_{3v} symmetry with a long Si–Cl bond kept frozen at 3.0794 Å. This localized structure is 8.6 kcal mol^{-1} *higher* in energy than **2a** (see Figure 2). The other Si–Cl bond contracts, but only slightly from 2.3592 Å in **2a** to 2.1967 Å in **2b** (see Figure 2). Note that the short C–Cl bond in the corresponding carbon system undergoes a more pronounced contraction from 2.3516 Å in **1a** to 1.8720 Å in **1b**.

Bonding in $Cl-AH_3-Cl^-$: To understand this difference in bonding capabilities of carbon and silicon, we have analyzed the energy and bonding in $ClCH_3Cl^-$ (**1**) and $ClSiH_3Cl^-$ (**2**) along a localization mode proceeding from the D_{3h}-symmetric pentavalent species **1a** and **2a** towards the corresponding localized structures. This was done by expanding one of the Cl–A bonds in steps of 0.05 Å from about 2.36 Å (**1a**: 2.3516 Å; **2a**: 2.3592 Å) to 2.5 Å, while allowing the remaining geometry parameters to relax, in particular, the other A–Cl bond which then contracts (i.e., localizes). The bonding in **1** and **2** was then examined along this localization mode by constructing the species stepwise from smaller molecular or atomic fragments and analyzing the bonding mechanism associated with bringing these fragments together. This can be done in various ways. Here, we present three variants that shed light onto the bonding in **1** and **2** from different, complementary perspectives. The results of the various analyses are collected in Figure 3.

First, we built $Cl-AH_3-Cl^-$ stepwise from the central atom $A^{''''}$ in its sp^3 valence state interacting with the $Cl_2^{-\bullet}$ fragment of the two axial substituents [see Eq. (1a)], followed by putting the resulting $Cl-A-Cl^{-'''}$ together with the $H_3^{'''}$ fragment of the three equatorial substituents [see Eq. (1b) and Figure S1 in the Supporting Information].

$$A^{''''} + Cl_2^{-\bullet} \rightarrow Cl-A-Cl^{-'''} \quad (1a)$$

$$Cl-A-Cl^{-'''} + H_3^{'''} \rightarrow Cl-AH_3-Cl^- \quad (1b)$$

Alternatively, we built $Cl-AH_3-Cl^-$ by first combining the central atom $A^{''''}$ with the $H_3^{'''}$ fragment of the three equatorial fragments [Eq. (2a)] and *then* put the resulting $AH_3^{\bullet}$ together with the $Cl_2^{-\bullet}$ fragment of the two axial substituents [see Eq. (2b) and Figure S2 in the Supporting Information).

$$A^{''''} + H_3^{'''} \rightarrow AH_3^{\bullet} \quad (2a)$$

$$AH_3^{\bullet} + Cl_2^{-\bullet} \rightarrow Cl-AH_3-Cl^- \quad (2b)$$

The third variant was the construction of $Cl-AH_3-Cl^-$ from the $H_3^{'''}$ fragment of the three equatorial substituents interacting with the $Cl_2^{-\bullet}$ fragment of the two axial substituents [see Eq. (3a)] and to put, thereafter, the central atom $A^{''''}$ into the resulting "cage" or "box" of substituents $Cl-H_3-Cl^{-''''}$ [see Eq. (3b) and Figure S3 in the Supporting Information].

$$H_3^{'''} + Cl_2^{-\bullet} \rightarrow Cl-H_3-Cl^{-''''} \quad (3a)$$

$$A^{''''} + Cl-H_3-Cl^{-''''} \rightarrow Cl-AH_3-Cl^- \quad (3b)$$

Note that all fragments in Equations (1)–(3) are in the valence configuration they adopt in the overall molecule and that unpaired electrons within one fragment are of the same spin, whereas unpaired electrons on two different fragments are of opposite spin in order to enable the formation of the electron-pair bonds. Also note that in all three fragmentation modes, the fragments $Cl_2^{-\bullet}$ and $H_3^{'''}$ occur, which have been constructed from Cl^- interacting with $Cl^{\bullet}$ and from three $H^{\bullet}$ atoms, respectively (see also Figure S4 in the Supporting Information).

The left panel of Figure 3 shows the analysis results for the three fragmentation modes of $ClCH_3Cl^-$ (**1**); the right panel shows the results for $ClSiH_3Cl^-$ (**2**). To highlight the equivalence of the two A–Cl bonds, we show the evolution of all energy components from one localized starting point (with, say, the left A–Cl = 2.5 Å) to the D_{3h}-symmetric, hypervalent species (both A–Cl ≈ 2.36 Å) to the other localized structure (with, say, the right A–Cl = 2.5 Å). Based on the symmetry of the process, the right half of the graphs was obtained as the mirror image of the left half. Energies are shown relative to the localized structures (A–Cl = 2.5 Å). In other words, the graphs show how the total energies of $ClCH_3Cl^-$ and $ClSiH_3Cl^-$ (black lines, designated "total") as well as all of the components associated with the steps

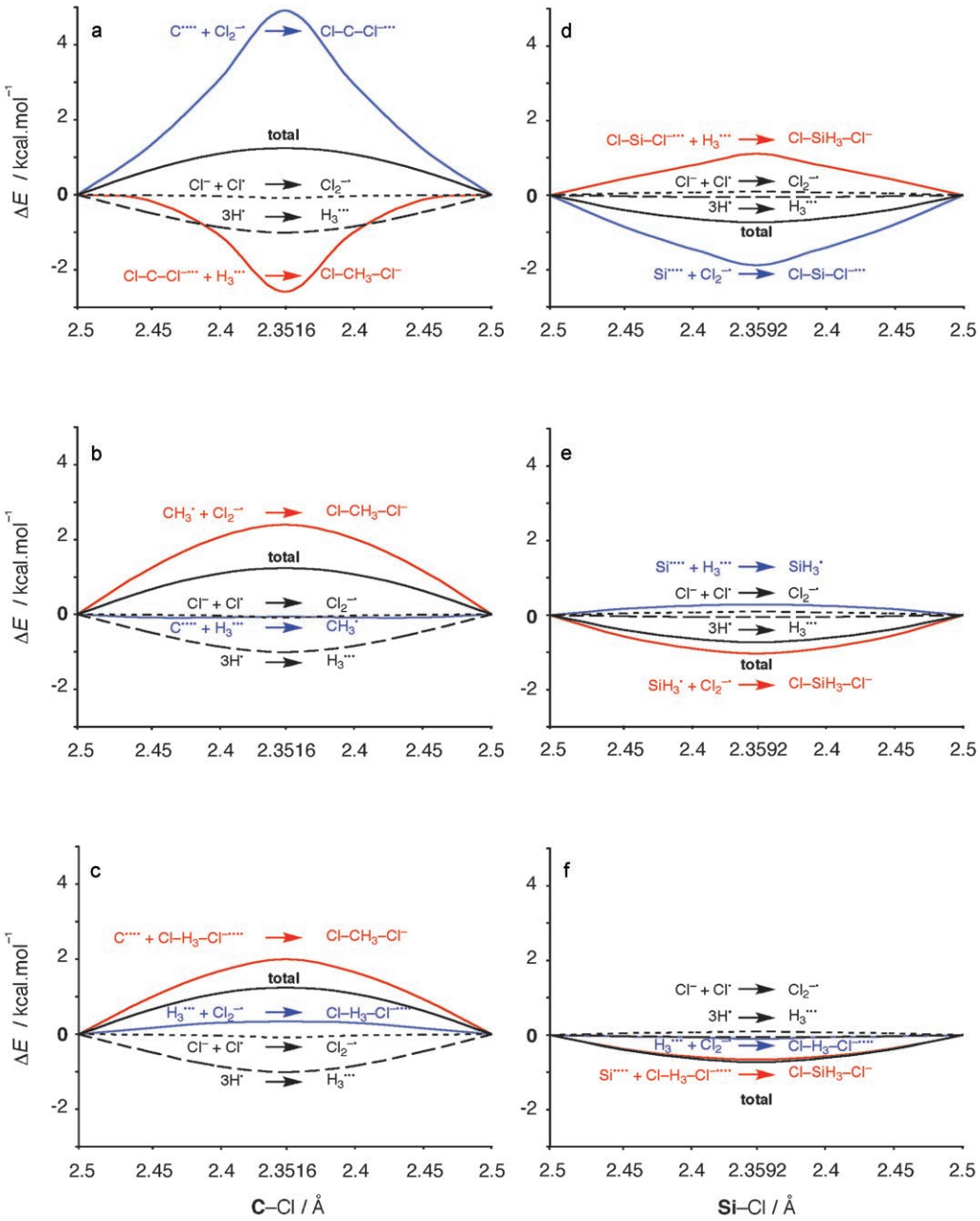

Figure 3. Three different decompositions (as indicated by partial reactions in a–c for carbon, and in d–f for silicon) of the relative energy (bold black line, designated "total") of $[ClCH_3Cl]^-$ and $[ClSiH_3Cl]^-$ along an S_N2-type deformation coordinate that brings the species from a localized C_{3v} structure via a D_{3h}-symmetric and pentavalent species to the other localized structure. The deformation coordinate is defined by stepwise varying one C–Cl (or Si–Cl) bond from 2.5 to 2.3516 Å (or 2.3592 Å) and optimizing all other geometric parameters in every step.

defined in Equations (1)–(3) (colored and dashed lines) change relative to the localized starting point with A–Cl = 2.5 Å.

Firstly, we note that the analyses reproduce a convex total energy profile for carbon (see Figure 3a–c) and a concave total-energy surface for silicon as the central atom (see Figure 3d–f).[27] Note that these total energy profiles are identical *within* the set of three graphs for **1** and *within* the set of three graphs for **2**. So are, of course, the energy curves associated with the formation of $Cl_2^{-\bullet}$ from $Cl^- + Cl^\bullet$ and those for the formation of $H_3^{\bullet\bullet\bullet}$ from three $H^\bullet$ (see Figure S4 in the Supporting Information).

The latter are comparatively shallow, especially for $ClSiH_3Cl^-$, and are not decisive for the key difference between **1** and **2**, in other words the convex and concave shape, respectively, of the total energy curve. The $Cl_2^{-\bullet}$ curve (short dashes) is, in fact, nearly constant because the overall Cl–Cl distance is large and changes little as the contraction of one A–Cl bond always occurs with the expansion of the other A–Cl bond. The $H_3^{\bullet\bullet\bullet}$ curve (long dashes) is

always stabilized at the symmetric, hypervalent structure. This is due to the fact that the AH_3 moiety goes from a pyramidal to a planar configuration in which the hydrogen atoms are slightly further away from each other and, therefore, experience less mutual steric (Pauli) repulsion.[28] This effect is much more pronounced for $ClCH_3Cl^-$ than for $ClSiH_3Cl^-$ because the hydrogen atoms in the former are in closer proximity due to the shorter C–H as compared to Si–H bonds.[28]

Thus, the origin of **1a** being a transition state and **2a** a stable, hypervalent species is located somewhere in the other interaction steps, in the two steps (a) and (b) defined in each of the Equations 1–3 (see blue and red curves, respectively, in Figure 3). A closer inspection shows that in each of the three fragmentation modes, the convex (**1**) or concave (**2**) nature of the total energy curve is determined by the interaction of the central moiety (either A or AH_3) with the axial substituents (or all substituents simultaneously).

The effect as such and the difference between **1** and **2** are most pronounced for fragmentation mode number one. As defined in Equation (1) and as can be seen in Figure 3a,d, the interaction between carbon and the axial-substituent fragment in the Cl–C–Cl$^{-\bullet\bullet\bullet}$ moiety of **1** is *destabilized* by nearly 5 kcal mol^{-1} as we go from the localized (C–Cl = 2.5 Å) to the symmetric, pentacoordinate structure **1a** (C–Cl ≈2.36 Å), whereas the corresponding change in the interaction between silicon and the axial-substituent fragment in the Cl–Si–Cl$^{-\bullet\bullet\bullet}$ moiety of **2** shows a *stabilization* of −1.88 kcal mol^{-1}. Note that this behavior is counteracted, but not overruled, by the destabilization in the interaction with the equatorial $H_3^{\bullet\bullet\bullet}$ substituents (consistent with the findings in reference [28]).

Bonding in Cl–A–Cl$^{-\bullet\bullet\bullet}$: The fact that Cl–C–Cl$^{-\bullet\bullet\bullet}$ is labile with respect to bond localization is interesting. This species consists of three main group atoms with a 3c-4e bonding mechanism based on p_σ AOs (see Scheme 1). It is not only isostructural, but also isoelectronic with the linear trihalides X–Y–X$^-$ which are known to adopt a delocalized, hypervalent structure of $D_{\infty h}$ symmetry.[21] In particular, Cl–F–Cl$^-$ which, just as Cl–C–Cl$^{-\bullet\bullet\bullet}$, consists of an arrangement of two terminal chlorine atoms and a central second period atom, is a stable $D_{\infty h}$-symmetric species with two equivalent Cl–F bonds (2.0782 Å) at the BP86/TZ2P level used in this investigation.

To further investigate this issue, we have computed the equilibrium geometries of Cl–C–Cl$^{-\bullet\bullet\bullet}$ (**3a**) and Cl–Si–Cl$^{-\bullet\bullet\bullet}$ (**4a**). Both species were found to posses linear, $D_{\infty h}$-symmetric equilibrium geometries with C–Cl and Si–Cl bond lengths of 1.9784 Å (**3a**) and 2.2804 Å (**4a**), respectively (see Figure 4). Comparison with the corresponding C–Cl and Si–Cl distances in the pentacoordinate $ClCH_3Cl^-$ (**1a**) and $ClSiH_3Cl^-$ (**2a**) leads to a striking observation: the Si–Cl bond is not much different for the dicoordinate silicon in **4a** (2.2804 Å) than for the pentacoordinate silicon in **2a** (2.3592 Å); from the former to the latter, it expands by only

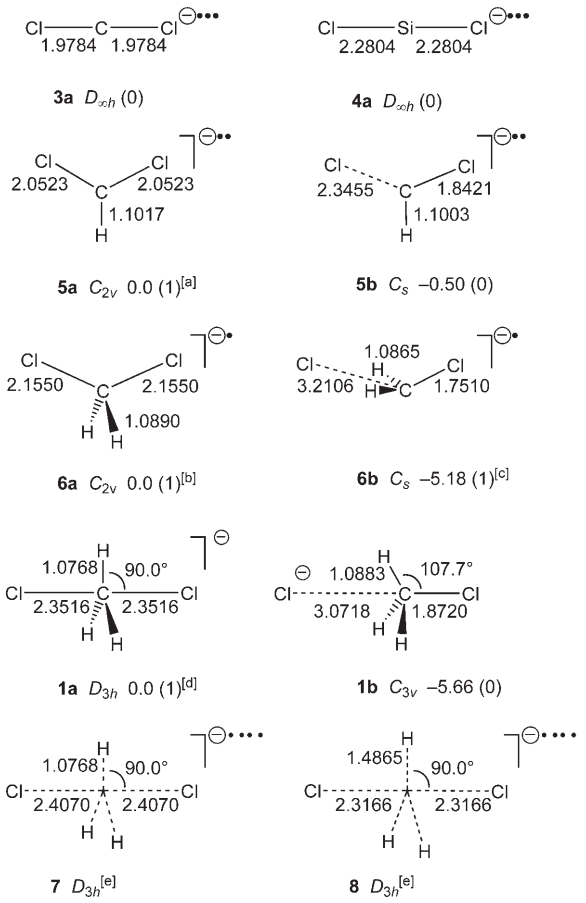

Figure 4. Geometries (in Å, °), relative energies (in kcal mol^{-1}) and number of imaginary frequencies (in parentheses) of selected $ClCH_nCl^{-(3-n)\bullet}$ structures with $n = 0$, 1, 2, and 3 (i.e. **3a**, **5**, **6**, and **1**, respectively), $ClSiCl^{-3\bullet}$ (**4a**) and $ClH_3Cl^{-\bullet\bullet\bullet\bullet}$ "boxes" of substituents (i.e. **7** and **8**), computed at BP86/TZ2P. [a] *i*198 cm^{-1}, [b] *i*271 cm^{-1}, [c] *i*111 cm^{-1}, [d] *i*316 cm^{-1}, and [e] optimized with frozen H_3 moiety (see text).

0.0788 Å or 3% (compare Figure 2 and Figure 4). At variance, the C–Cl bond expands by a sizeable 0.3732 Å or 19% (!) if we go from dicoordinate carbon in **3a** (1.9784 Å) to pentacoordinate carbon in **1a** (2.3516 Å). Consequently, the C–Cl and Si–Cl bonds in **1a** and **2a** are in good approximation of equal length, as has already been mentioned.

Thus, in **1a**, the axial chlorine substituents *cannot* approach the central carbon atom closely enough to form the intrinsically optimal C–Cl bonds for the Cl–C–Cl$^{-\bullet\bullet\bullet}$ moiety. In contrast, in **2a** the axial chlorine substituents *can* approach the central silicon atom closely enough to form the intrinsically optimal Si–Cl bonds for the Cl–Si–Cl$^{-\bullet\bullet\bullet}$ moiety. Consequently, the carbon atom in the Cl–C–Cl$^{-\bullet\bullet\bullet}$ fragment of **1a** moves closer to one of the two chlorine atoms to form one strong C–Cl bond at the expense of sacrificing one weak C–Cl bond. This is not necessary for the Cl–Si–Cl$^{-\bullet\bullet\bullet}$ fragment of **2a** in which the Si–Cl bonds already nearly have their optimal value.

This is nicely illustrated by Figure 5, which shows how the interaction between A$^{\bullet\bullet\bullet}$ and $Cl_2^{-\bullet}$ (the black line, designated

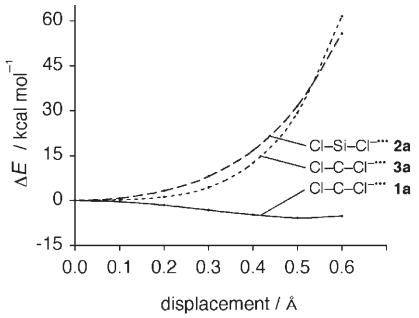

Figure 5. Interaction energy between central atom A··· and terminal substituents $Cl_2^{-\cdot}$ for three Cl–A–Cl⁻··· fragments as a function of the displacement of A towards one of the Cl atoms with the Cl–Cl distance kept frozen as shown in **IV**: a) Cl–C–Cl⁻··· fragment taken from transition state **1a**; b) Cl–Si–Cl⁻··· fragment taken from transition complex **2a**; c) optimized Cl–C–Cl⁻··· species **3a**.

"total") varies if the central atom A of a linear Cl–A–Cl⁻··· arrangement with a frozen Cl–Cl distance is displaced by 0.5 Å (in steps of 0.1 Å) from the central position towards one of the frozen terminal chlorine atoms (see **IV**).

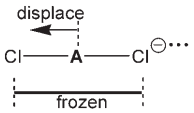

IV

This numerical experiment was carried out for: 1) Cl–C–Cl⁻··· with Cl–Cl = 2 × 2.3516 Å as in **1a**; 2) for Cl–Si–Cl⁻··· with Cl–Cl = 2 × 2.3592 Å as in **2a**; and 3) for Cl–C–Cl⁻··· with Cl–Cl = 2 × 1.9784 Å as in **3a**. For Cl–C–Cl⁻··· with the long Cl–Cl distance as in **1a**, the displacement of carbon away from the center and towards one of the chlorine atoms leads to a slight stabilization of −5.82 kcal mol^{-1} at a displacement of 0.5 Å (see Figure 5). Optimization for this frozen Cl–Cl distance yields a species with one C–Cl distance of 1.8285 Å and one of 2.8747 Å (not shown in the figures). In contrast, for Cl–Si–Cl⁻··· with the long Cl–Cl distance as in **2a**, the displacement of silicon away from the center and towards one of the chlorine atoms leads to a quite pronounced *destabilization* of +32 kcal mol^{-1} at a displacement of 0.5 Å. Once the Cl–Cl distance in Cl–C–Cl⁻··· adopts its intrinsically, that is, for the species **3a**, optimal and somewhat shorter value, the interaction energy varies in the same manner as for Cl–Si–Cl⁻···. It is destabilized by +29 kcal mol^{-1} at a displacement of 0.5 Å of the central carbon atom towards one of the terminal chlorine atoms.

The short C–Cl bond length of 1.9784 Å in the Cl–C–Cl⁻··· species **3a** and the longer one of 2.3592 Å in the Cl–Si–Cl⁻··· species **4a** concur nicely with the fact that the overlap between the more compact carbon $2p_z$ AO and the chloride $3p_z$ AO reaches its optimum of 0.270 at C–Cl = 1.88 Å, whereas the overlap between the more diffuse silicon $3p_z$ AO and chloride $3p_z$ AO reaches its optimum of 0.299 at a longer Si–Cl separation of 2.26 Å (see also orbital contour plots in Figure S5 in the Supporting Information). Note that the optimum $\langle 2p_z|3p_z\rangle$ and $\langle 3p_z|3p_z\rangle$ distances are shorter than the actual optimum C–Cl and Si–Cl distances in **3a** and **4a**. This is, of course, due to the fact that the 3c-4e bonding in these species is somewhat more involved than in a diatomic species and because Pauli repulsion with closed valence and core shells of the other atoms produces a longer equilibrium distance compared to the fictitious situation with only bonding orbital interactions.[29]

The central atom as a ball-in-a-"box" of substituents: As a result of the "too long" and weak C–Cl bonds in D_{3h}-symmetric $ClCH_3Cl^-$ (**1a**), the system has the propensity to localize and strengthen one of the bonds at the expense of breaking the other one. But why are the C–Cl bonds in **1a** too long in the first place; 2.3516 Å instead of the 1.9784 Å which would be optimal for the isolated Cl–C–Cl⁻··· unit?

To answer this question, we added the three hydrogen atoms to the substituents fragment, as the long C–Cl distances occur in the presence of these equatorial substituents. This yields the complete "box" of substituents Cl–H_3–Cl⁻···. This corresponds to step 1 of the fragmentation scheme defined in Equation (3). This box is as such not a stable species, but it does adopt an optimum geometry under constrained optimization with C_{3v} symmetry and a frozen H_3 unit. Interestingly, this yields a Cl–H_3–Cl⁻··· structure that is very similar to the corresponding fragments in **1a** and **2a**: The distance between the Cl atoms and the empty central site (where otherwise C or Si are located) amounts to 2.4070 and 2.3166 Å in **7** and **8** in which the H_3 unit is taken from **1a** and **2a**, respectively (see Figure 4). This can be compared to the nearly identical C–Cl and Si–Cl bond lengths of 2.3516 and 2.3592 Å in **1a** and **2a** (see Figure 2).

The above finding is important because the box of substituents has an intrinsic optimum at the A–Cl distances of about 2.36 Å, which is also found in **1a** and **2a**. Further compressing the box increases its energy, although the associated potential-energy surface (PES) is relatively shallow. This can be nicely recognized in a computational experiment in which the axial chlorine substituents of the Cl–H_3–Cl⁻··· box are symmetrically compressed (preserving the D_{3h} symmetry) in steps of 0.1 Å from a distance of 2.5 to 1.9 Å with a frozen H_3 unit as shown in **V**.

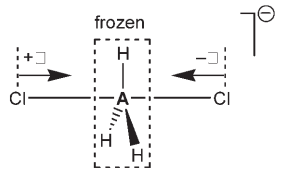

V

The results are depicted in Figure 6 with the carbon and silicon systems to the left and to the right, respectively. Along the compression, the substituent–substituent interaction in the box goes through a minimum at 2.3–2.4 Å and is then destabilized as the Cl–H distance is further reduced (see Figure 6, red lines, carbon and silicon examples are left and right, respectively). This resistance towards compression

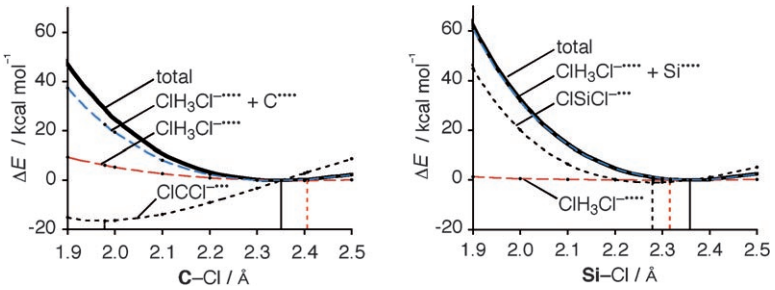

Figure 6. Energy of D_{3h}-symmetric $ClCH_3Cl^-$ (left) and $ClSiH_3Cl^-$ (right) relative to the transition state **1a** and transition complex **2a**, respectively, as a function of the Cl–Cl distance (see also **V**), computed at BP86/TZ2P. Relative energies of the overall species $ClAH_3Cl^-$ (bold lines, designated "total") are decomposed into the relative energy of the "box" of substituent $Cl–H_3–Cl^{····}$ (red dashed lines) plus the interaction between this "box" and the central atom A (blue dashed lines). Furthermore, the relative energies of $Cl–C–Cl^{····}$ (left) and $Cl–Si–Cl^{····}$ (right) are indicated (black dashed lines). Vertical lines indicate the energy minimum for the corresponding energy curve.

is, of course, greatly increased if the central atom is introduced into the overall $ClAH_3Cl^-$ systems (bold black lines in Figure 6). This is due to Cl–C or Cl–Si repulsion (in addition to the Cl–H repulsion), which destabilizes the interaction between the central atom and the axial substituents at shorter distances (blue lines in Figure 6). Thus, steric factors prevent the box of substituents from getting more compact than in either **1a** or **2a**, even in the absence of the central atom, yielding substituent boxes of very similar geometrical dimensions for both carbon and silicon (see Figures 2 and 4).

The optimum "box size" of the silicon species (Figure 6, right) is more or less the same for the isolated box $Cl–H_3–Cl^{····}$ (red vertical line), for the interaction of $A^{····}$ + $Cl–H_3–Cl^{····}$, and for the overall system $Cl–SiH_3–Cl^-$ (black vertical line). Interestingly, it is also more or less the same for the $Cl–Si–Cl^{····}$ species (dashed black vertical line). Thus, both steric factors and Si–Cl bonding interactions ("electronic factors") favor a substituent box of approximately the same size leading to a stable symmetric structure **2a** for $ClSiH_3Cl^-$.

The situation is qualitatively different for the carbon species (Figure 6, left). The optimum "box size" is still more or less the same for the isolated box $Cl–H_3–Cl^{····}$ (red vertical line), for the interaction of $A^{····}$ + $Cl–H_3–Cl^{····}$, and for the overall system $Cl–CH_3–Cl^-$ (black vertical line). Strikingly, although in agreement with the above analyses of the $Cl–A–Cl^{····}$ species, the optimum "box size" here is at much shorter Cl–Cl distances for the $Cl–C–Cl^{····}$ species (dashed black vertical line). We recall that the energy curves in Figure 6 refer to symmetric Cl–Cl variation and not to localization modes as shown in Figures 3 and 5. The consequence of the counteracting tendencies in $Cl–CH_3–Cl^-$ of having a large $Cl–H_3–Cl^{····}$ but striving for short C–Cl bonds in $Cl–C–Cl^{····}$ is that, if one lifts this symmetry constraint, the C–Cl bonds localize while, simultaneously, the size of the $Cl–H_3–Cl^{····}$ box is more or less preserved. In keeping with this, optimization of the $ClCH_3Cl^-$ structure **1a** with a frozen [$Cl–H_3–Cl$] moiety but an unconstrained carbon atom yields a localized structure at -1.2 kcal mol^{-1} with C–Cl bond lengths of 2.09 and 2.61 Å. Thus, whereas steric factors still lead to a large substituent box, C–Cl bonding interactions ("electronic factors") favor shorter C–Cl bond lengths leading to the localized structure **1b** for $ClCH_3Cl^-$.

The qualitative picture that emerges from our MO analyses is that the five substituents form a cage or "box" ClH_3Cl^- in which they are in mutual steric contact (Scheme 2). The central atom A can be viewed as a "ball" in that box. Silicon fits nearly exactly into the box and can bind simultaneously to the top and the bottom (Scheme 2). This yields the hypervalent $ClSiH_3Cl^-$ with a trigonal bipyramidal structure. At variance, the carbon atom is too small to touch both the top and the bottom and it can thus only bind to one of them (Scheme 2). This leads to a species $Cl^-\cdots H_3CCl$ with one localized C–Cl bond, one long C–Cl contact, and a pyramidalized CH_3 unit.

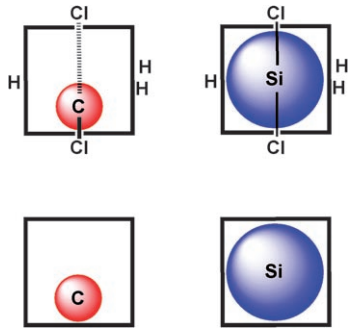

Scheme 2. "Ball-in-a-box" model for five-coordinate carbon and silicon

We have generalized our findings for $ClCH_3Cl^-$ and $ClSiH_3Cl^-$ to other Group 14 central atoms (Ge, Sn, and Pb) and axial substituents (F); the data are collected in Table S1 of the Supporting Information. The D_{3h}-symmetric moieties FCH_3F^- and $FSiH_3F^-$ are a labile transition state and a stable trigonal bipyramidal complex, respectively. In good agreement with the above analyses, we again found that the C–F bond length in D_{3h}-symmetric FCH_3F^- (1.8538 Å) is much longer than its intrinsic optimum as given by the $D_{\infty h}$-symmetric equilibrium structure of $F–C–F^{····}$ (1.5937 Å). Furthermore, all of the heavier $ClAH_3Cl^-$ analogues (A = Ge, Sn, Pb) have stable D_{3h}-symmetric equilibrium structures, just like $ClSiH_3Cl^-$. The A–Cl bond lengths in D_{3h}-symmetric $ClAH_3Cl^-$ (2.4928, 2.6208, and 2.7346 Å for A = Ge, Sn, Pb, respectively) are quite close to its intrinsic optimum as given by the $D_{\infty h}$-symmetric

equilibrium structure of Cl–A–Cl$^{\cdots}$ (2.4048, 2.5758, and 2.7184 Å for A = Ge, Sn, Pb, respectively), which agrees well with our analyses described above.

Finally, the ball-in-a-box model also stresses an important difference between the issue of (non)hypervalence, in C versus Si, and the issue of (anti)aromaticity, in benzene versus 1,3-cylobutadiene. Both concepts deal with the propensity of a system to localize or delocalize bonds; however, the question of whether a species is aromatic or antiaromatic is a purely electronic problem (i.e. determined by bonding orbital interactions)[30] whereas steric factors (i.e. Pauli repulsive orbital interactions) play a key role in the question if an atom has the capability to form stable hypervalent structures with its substituents or not.

Nucleophilic substitution at carbon without a barrier: The ball-in-a-box model further consolidates earlier reports that highlight the steric nature of the central barrier in S_N2 reactions.[16a,b] This has prompted us to carry out one additional computational experiment. If steric congestion around the central atom plays a prominent role, the central S_N2 barrier should be lowered if we reduce the number of substituents. Indeed, this is exactly what happens in the series of nucleophilic substitutions at carbon (S_N2@C) in the series of model reactions shown in Equations (4a)–(4d).

$$Cl^- + CH_3Cl \rightarrow ClCH_3 + Cl^- \quad (4a)$$

$$Cl^- + CH_2Cl^{\cdot} \rightarrow ClCH_2^{\cdot} + Cl^- \quad (4b)$$

$$Cl^- + CHCl^{\cdot\cdot} \rightarrow ClCH^{\cdot\cdot} + Cl^- \quad (4c)$$

$$Cl^- + CCl^{\cdot\cdot\cdot} \rightarrow ClC^{\cdot\cdot\cdot} + Cl^- \quad (4d)$$

In reactions shown in Equations (4a)–(4d), the number of equatorial hydrogen substituents in the transition structure decreases from $n = 3$ to 2 to 1 to 0 (for a, b, c, and d, respectively). And, as expected, the barrier decreases systematically from 5.7 to 5.2 to 0.5 to 0 kcal mol^{-1} (see Figure 4). Furthermore, consistent with the systematic reduction in barrier height, the C–Cl bonds in the symmetric transition structure contract from 2.3516 (**1a**) to 2.1550 (**6a**) to 2.0523 (**5a**) to 1.9784 Å (**3a**), as can be seen in Figure 4.

Conclusion

Based on quantitative MO theory, we have developed the qualitative "ball-in-a-box" model for understanding why certain atoms A (such as silicon) can form stable hypervalent configurations $ClAH_3Cl^-$, while others (such as carbon) cannot. The qualitative picture that emerges from our MO analyses is that the five substituents form a cage or "box" ClH_3Cl^- in which they are in mutual steric contact (if the substituents are forced at a closer mutual distance, they begin to strongly repel each other). The central atom A can be viewed as a "ball" in that box.

Silicon fits nearly exactly into the box and can bind simultaneously to the top and the bottom. This yields the hypervalent $ClSiH_3Cl^-$ with a trigonal bipyramidal structure. At variance, the carbon atom is too small to touch both the top and the bottom, and it can thus only bind to one of them. To somewhat stretch the qualitative picture, one could say that the carbon atom ball "drops" to the bottom of the box (Scheme 2), leading to a $Cl^-\cdots H_3CCl$ species with one localized C–Cl bond, one long C–Cl contact, and a pyramidalized CH_3 unit. Our findings for $ClCH_3Cl^-$ and $ClSiH_3Cl^-$ have been generalized to other group 14 central atoms (Ge, Sn, and Pb) and another axial substituent (F). The ball-in-a-box model is supported further by the fact that the S_N2 central barrier for nucleophilic attack by Cl^- decreases monotonically along the substrates CH_3Cl, $^{\cdot}CH_2Cl$, $^{\cdot\cdot}CHCl$, and $^{\cdot\cdot\cdot}CCl$.

In a sense, the ball-in-a-box model allows MO theory to catch up with VB theory regarding the treatment and understanding of the phenomenon of hypervalence. It also nicely integrates bonding orbital interactions ("electronic factors") and repulsive orbital interactions ("steric factors") into one qualitative model. This highlights the importance of the relative size of the central atom for the capability to form hypervalent compounds.[4,13,15]

Acknowledgement

We thank the Netherlands Organization for Scientific Research (NWO-CW and NWO-NCF) and the National Research School Combination for Catalysis (NRSC-C) for financial support.

[1] G. N. Lewis, *J. Am. Chem. Soc.* **1916**, *38*, 762.
[2] a) K. Y. Akiba in *Chemistry of Hypervalent Compounds* (Ed.: K. Y. Akiba), Wiley-VCH, Weinheim, **1998**, Chapters 1 and 2; b) C. Chuit, R. J. P. Corriu, C. Reye in *Chemistry of Hypervalent Compounds* (Ed.: K. Y. Akiba), Wiley-VCH, Weinheim, **1998**, Chapter 4.
[3] a) R. Hoffmann, *Solids and Surfaces: A Chemist's View of Bonding in Extended Structures*, Wiley, New York, **1989**; b) J. I. Musher, *Angew. Chem.* **1969**, *81*, 68; *Angew. Chem. Int. Ed. Engl.* **1969**, *8*, 54; c) L. Pauling, *The Nature of the Chemical Bond*, 3rd ed., Cornell University Press, Ithaca, New York, **1960**.
[4] a) S. Noury, B. Silvi, R. J. Gillespie, *Inorg. Chem.* **2002**, *41*, 2164; b) R. J. Gillespie, E. A. Robinson, *Inorg. Chem.* **1995**, *34*, 978.
[5] J. Cioslowski, S. T. Mixon, *Inorg. Chem.* **1993**, *32*, 3209.
[6] a) M. B. Smith, J. March, *Advanced Organic Chemistry: Reactions, Mechanisms and Structure*, Wiley-Interscience, New York, **2001**; b) F. A. Carey, R. J. Sundberg, *Advanced Organic Chemistry: Structure And Mechanisms (Part A)*, Springer, New York, **2000**; c) A. Streitwieser, C. H. Heathcock, E. M. Kosower, *Introduction to Organic Chemistry* , Prentice Hall, Paramus, **1998**.
[7] a) K. Y. Akiba, Y. Moriyama, M. Mizozoe, H. Inohara, T. Nishii, Y. Yamamoto, M. Minoura, D. Hashizume, F. Iwasaki, N. Takagi, K. Ishimura, S. Nagase, *J. Am. Chem. Soc.* **2005**, *127*, 5893; b) Y. Yamamoto, K. Y. Akiba, *J. Synth. Org. Chem. Jpn.* **2004**, *62*, 1128; c) K. Y. Akiba, M. Yamashita, Y. Yamamoto, S. Nagase, *J. Am. Chem. Soc.* **1999**, *121*, 10644; d) G. A. Olah, G. K. S. Prakash, R. E. Williams, L. D. Field, K. Wade, *Hypercarbon Chemistry*, Wiley, New York, **1987**; e) T. R. Forbus, J. C. Martin, *J. Am. Chem. Soc.* **1979**, *101*, 5057.
[8] J. C. Martin, *Science* **1983**, *221*, 509.
[9] D. J. Hajdasz, R. R. Squires, *J. Am. Chem. Soc.* **1986**, *108*, 3139.

[10] a) G. L. Gutsev, *Chem. Phys. Lett.* **1991**, *184*, 305; b) W. C. Hamilton, *Acta Crystallogr.* **1962**, *15*, 353.
[11] a) J. K. Laerdahl, E. Uggerud, *Int. J. Mass Spectrom.* **2002**, *214*, 277; b) M. N. Glukhovtsev, A. Pross, L. Radom, *J. Am. Chem. Soc.* **1996**, *118*, 6273; c) M. N. Glukhovtsev, A. Pross, L. Radom, *J. Am. Chem. Soc.* **1995**, *117*, 2024; d) S. S. Shaik, H. B. Schlegel, S. Wolfe, *Theoretical Aspects of Physical Organic Chemistry: the S_N2 Mechanism*, Wiley, New York, **1992**; e) G. L. Gutsev, *Chem. Phys.* **1992**, *166*, 57; f) Z. Shi, R. J. Boyd, *J. Phys. Chem.* **1991**, *95*, 4698; g) R. Vetter, L. Zulicke, *J. Am. Chem. Soc.* **1990**, *112*, 5136; h) S. C. Tucker, D. G. Truhlar, *J. Phys. Chem.* **1989**, *93*, 8138; i) S. Wolfe, D. J. Mitchell, H. B. Schlegel, *J. Am. Chem. Soc.* **1981**, *103*, 7692; j) J. D. Payzant, K. Tanaka, L. D. Betowski, D. K. Bohme, *J. Am. Chem. Soc.* **1976**, *98*, 894; k) F. Keil, R. Ahlrichs, *J. Am. Chem. Soc.* **1976**, *98*, 4787; l) R. F. W. Bader, A. J. Duke, R. R. Messer, *J. Am. Chem. Soc.* **1973**, *95*, 7715; m) A. Dedieu, A. Veillard, *J. Am. Chem. Soc.* **1972**, *94*, 6730; n) C. D. Ritchie, G. A. Chappell, *J. Am. Chem. Soc.* **1970**, *92*, 1819.
[12] W. N. Olmstead, J. I. Brauman, *J. Am. Chem. Soc.* **1977**, *99*, 4219.
[13] M. J. S. Dewar, E. Healy, *Organometallics* **1982**, *1*, 1705.
[14] a) G. L. Gutsev, *J. Phys. Chem.* **1994**, *98*, 1570; b) M. T. Carroll, M. S. Gordon, T. L. Windus, *Inorg. Chem.* **1992**, *31*, 825; c) S. Gronert, R. Glaser, A. Streitwieser, *J. Am. Chem. Soc.* **1989**, *111*, 3111; d) N. T. Anh, C. Minot, *J. Am. Chem. Soc.* **1980**, *102*, 103; e) P. Baybutt, *Mol. Phys.* **1975**, *29*, 389; f) F. Keil, R. Ahlrichs, *Chem. Phys.* **1975**, *8*, 384; g) D. L. Wilhite, L. Spialter, *J. Am. Chem. Soc.* **1973**, *95*, 2100.
[15] A. E. Reed, P. von R. Schleyer, *Chem. Phys. Lett.* **1987**, *133*, 553.
[16] a) A. P. Bento, F. M. Bickelhaupt, *J. Org. Chem.* **2007**, *72*, 2201; see also: b) M. A. van Bochove, M. Swart, F. M. Bickelhaupt, *J. Am. Chem. Soc.* **2006**, *128*, 10738; c) A. P. Bento, M. Solà, F. M. Bickelhaupt, *J. Comput. Chem.* **2005**, *26*, 1497.
[17] a) G. te Velde, F. M. Bickelhaupt, S. J. A. van Gisbergen, C. Fonseca Guerra, E. J. Baerends, J. G. Snijders, T. Ziegler, *J. Comput. Chem.* **2001**, *22*, 931; b) C. Fonseca Guerra, O. Visser, J. G. Snijders, G. te Velde, E. J. Baerends in *Methods and Techniques for Computational Chemistry* (Eds.: E. Clementi, G. Corongiu), STEF, Cagliari, **1995**, p. 305–395; c) E. J. Baerends, D. E. Ellis, P. Ros, *Chem. Phys.* **1973**, *2*, 41; d) E. J. Baerends, P. Ros, *Chem. Phys.* **1975**, *8*, 412; e) E. J. Baerends, P. Ros, *Int. J. Quantum Chem. Quantum. Chem. Symp.* **1978**, *12*, 169; f) C. Fonseca Guerra, J. G. Snijders, G. te Velde, E. J. Baerends, *Theor. Chem. Acc.* **1998**, *99*, 391; g) P. M. Boerrigter, G. te Velde, E. J. Baerends, *Int. J. Quantum Chem.* **1988**, *33*, 87; h) G. te Velde, E. J. Baerends, *J. Comput. Phys.* **1992**, *99*, 84; i) J. G. Snijders, E. J. Baerends, P. Vernooijs, *At. Data Nucl. Data Tables* **1982**, *26*, 483; j) J. Krijn, E. J. Baerends, *Fit-Functions in the HFS-Method; Internal Report (in Dutch)*, Vrije Universiteit, Amsterdam, **1984**; k) L. Versluis, T. Ziegler, *J. Chem. Phys.* **1988**, *88*, 322; l) J. C. Slater, *Quantum Theory of Molecules and Solids, Vol. 4*, McGraw-Hill, New York, **1974**; m) A. D. Becke, *J. Chem. Phys.* **1986**, *84*, 4524; n) A. Becke, *Phys. Rev. A* **1988**, *38*, 3098; o) S. H. Vosko, L. Wilk, M. Nusair, *Can. J. Phys.* **1980**, *58*, 1200; p) J. P. Perdew, *Phys. Rev. B* **1986**, *33*, 8822 (Erratum: Phys. Rev. B **1986**, 34, 7406); q) L. Fan, T. Ziegler, *J. Chem. Phys.* **1991**, *94*, 6057; r) E. van Lenthe, E. J. Baerends, J. G. Snijders, *J. Chem. Phys.* **1994**, *101*, 9783.
[18] a) "Kohn-Sham Density Functional Theory: Predicting and Understanding Chemistry": F. M. Bickelhaupt, E. J. Baerends, *Rev. Comput. Chem.* **2000**, *15*, 1; for the analysis of electron-pair (2c-2e) bonds see: b) F. M. Bickelhaupt, N. M. M. Nibbering, E. M. van Wezenbeek, E. J. Baerends, *J. Phys. Chem.* **1992**, *96*, 4864; for the analysis of 2c-3e bonds see: c) F. M. Bickelhaupt, A. Diefenbach, S. V. de Visser, L. J. de Koning, N. M. M. Nibbering, *J. Phys. Chem. A* **1998**, *102*, 9549.
[19] R. Hoffmann, J. M. Howell, E. L. Muetterties, *J. Am. Chem. Soc.* **1972**, *94*, 3047.
[20] a) G. C. Pimentel, *J. Chem. Phys.* **1951**, *19*, 446; b) R. J. Hach, R. E. Rundle, *J. Am. Chem. Soc.* **1951**, *73*, 4321.
[21] G. A. Landrum, N. Goldberg, R. Hoffmann, *J. Chem. Soc. Dalton Trans.* **1997**, 3605.
[22] a) C. A. Ramsden, *Chem. Soc. Rev.* **1994**, *23*, 111; b) T. A. Albright, J. K. Burdett, M.-H. Whangbo, *Orbital Interactions in Chemistry*, Wiley, New-York, **1985**.
[23] a) F. M. Bickelhaupt, M. Sola, P. von R. Schleyer, *J. Comput. Chem.* **1995**, *16*, 465; b) A. E. Reed, P. von R. Schleyer, *J. Am. Chem. Soc.* **1990**, *112*, 1434; c) E. Magnusson, *J. Am. Chem. Soc.* **1990**, *112*, 7940; d) W. Kutzelnigg, *Angew. Chem.* **1984**, *96*, 262; *Angew. Chem. Int. Ed. Engl.* **1984**, *23*, 272.
[24] a) S. Shaik, A. Shurki, *Angew. Chem.* **1999**, *111*, 616; *Angew. Chem. Int. Ed.* **1999**, *38*, 587; b) P. C. Hiberty, *J. Mol. Struct. (THEOCHEM)* **1998**, *451*, 237; c) G. Sini, G. Ohanessian, P. C. Hiberty, S. S. Shaik, *J. Am. Chem. Soc.* **1990**, *112*, 1407; d) G. Sini, P. C. Hiberty, S. S. Shaik, *J. Chem. Soc. Chem. Commun.* **1989**, 772.
[25] a) T. Ziegler, A. Rauk, *Inorg. Chem.* **1979**, *18*, 1755; b) T. Ziegler, A. Rauk, *Inorg. Chem.* **1979**, *18*, 1558; c) T. Ziegler, A. Rauk, *Theor. Chim. Acta* **1977**, *46*, 1.
[26] a) K. Kitaura, K. Morokuma, *Int. J. Quantum Chem.* **1976**, *10*, 325; b) K. Morokuma, *J. Chem. Phys.* **1971**, *55*, 1236.
[27] These energy profiles closely resemble but are not exactly identical to the minimum energy profiles corresponding to the internal reaction coordinate as defined in K. Fukui, *Acc. Chem. Res.* **1981**, *14*, 363.
[28] F. M. Bickelhaupt, T. Ziegler, P. von R. Schleyer, *Organometallics* **1996**, *15*, 1477.
[29] a) M. L. Munzarová, R. Hoffmann, *J. Am. Chem. Soc.* **2002**, *124*, 4787; b) F. M. Bickelhaupt, R. L. DeKock, E. J. Baerends, *J. Am. Chem. Soc.* **2002**, *124*, 1500.
[30] S. C. A. H. Pierrefixe, F. M. Bickelhaupt, *Chem. Eur. J.* **2007**, *13*, 6321.

Received: August 10, 2007
Published online: December 4, 2007

